Progress In Electromagnetics Research M, Vol. 115, 83–92, 2023

Tripartite Correlations in Quantum Radar and Communication Systems

Rory A. Bowell[1], Matthew J. Brandsema[1], Ram M. Narayanan[1, *], Stephen W. Howell[2], and Jonathan M. Dilger[2]

Abstract—Quantum-based systems are an emerging topic of research due to their potential for increasing performance in a variety of classical systems. In radar and communication systems, quantum technologies have been explored in an effort to increase the correlation performance in the low signal-to-noise ratio (SNR) regime. While this increase has been shown both mathematically and in the laboratory using bipartite states, systems utilizing multi-partite squeezing and entanglement may lead to an even further performance increase. We investigate this by analyzing the correlation coefficient for a tripartite system electric field measurement to determine how it compares to the bipartite systems in the current literature for the same transmit powers. This is done by defining a tripartite wave function in terms of the mean photon number per mode then determining the covariance matrix from this wave function. This work is important in understanding how alternative states of light can be used for quantum radar applications.

1. INTRODUCTION

Quantum radar has been a topic of interest in the field of quantum sensing in recent years due to various benefits over a classical system, in particular, the ability to achieve a higher correlation in the low signal-to-noise ratio regime. While these benefits have been demonstrated both through simulation [1–7] and in experiments [8–12], the lack of transmit power currently available for a two-photon entangled source limits the application of the technology. To date, almost all quantum radar analysis has been restricted to bipartite states, whereby the signal and idler beam have one photon originating from the pair produced during the generation process. These two-photon quantum radar systems work using spontaneous parametric down conversion. In this paper, we explore the possible benefits of using a tripartite state to perform ranging [13–16] by investigating whether the extra photon yields correlation benefits or other advantages of the return signal.

The current quantum radar design uses spontaneous parametric down conversion (SPDC) where one high energy photon is split into two photons of half the original energy. With this, one of the photons created is kept as an idler and the other is sent at the target as the signal. When the signal returns, a correlation method is used to determine if the returning photons are from the original signal. This bipartite quantum system has shown a 3-dB improvement in the error exponential which means that it has better detection in high noise environments [17–22]. Similarly to the two-photon method, the three-photon method looks to obtain a quantum advantage through the use of signal and idler beams. However, with the tripartite state we are able to transmit two signals that are correlated with a single idler. We believe that this arrangement with a single idler could lead to benefits in correlation performance in lossy channels. We seek to explore whether having more photons per generation leads to

Received 10 January 2023, Accepted 7 February 2023, Scheduled 18 February 2023
* Corresponding author: Ram M. Narayanan (rmn12@psu.edu).
[1] Department of Electrical and Computer Engineering, The Pennsylvania State University, University Park, PA, 16802, USA. [2] Naval Surface Warfare Center, Crane Division, 300 Highway 361, Crane, IN, 47522, USA.

correlation benefits of the returned beams. Conventional SPDC methods can only create equal photon number states on each branch of the photon generation, namely one photon each for the signal and idler, two photons each, three photons each, and so on [2]. These higher number states are increasingly less probable to generate and although they would possess more photons per generation, there would be less photons overall. A state specifically constructed to be tripartite (three-particles) can potentially alleviate this problem by using a different experimental setup entirely for the generation, keeping the same detection paradigm as bipartite systems, namely, storing or detecting the idler photon [1, 2, 23] and then later measuring the returned signal photons. However, in our tripartite case, each idler can correlate with *two* returning signal photons. In the setup described here, this would be done with a single detector for the signals and another detector to immediately detect the idler.

The ideas in this paper are based on our previous work, where we investigated immediate-idler-detection methods [2, 24]. To summarize, we found that one can obtain the same covariance expression using immediate idler detection, as obtained through joint measurement. This was done by measuring and correlating a large set of electric field measurements (bulk or quadrature). It is for this reason we choose to measure electric field in this paper. Number operator measurements led to very similar, but different values of covariance and correlation.

Here, we mathematically evaluate a tripartite radar system using a coupled three mode squeezed state introduced by Zhang and Glaser [25] which is generated through the use of an Rb atomic vapor and a four-wave-mixing process. For this calculation, we assume that the target is ideal (perfectly reflective). In this scheme, two lasers are used with non-linear crystals and one path from each of the signal idler pairs are mixed to create three part entanglement. In our evaluation, we solve for all parts of the covariance matrix and determine the covariance between the signal and idler beams for the system. Additionally, we simulate the correlation coefficient to be able to directly compare to the current literature. After we have determined the correlation coefficients of each of the path, we then compare it to the current bipartite system. To do this, we define a detection scheme for the tripartite system that will allow for an apples-to-apples comparison.

2. TRIPARTITE DERIVATION

The following tripartite derivation is made of two parts. First, we define the wave function in terms of the mean photon number per mode for each of the paths to allow for an easier comparison to transmit power. Secondly, the wave function in terms of the mean photon number per mode is used to derive the covariance matrix for the system.

2.1. Wave Function Derivation in Terms of Mean Photon Number Per Mode

We begin with a coupled three-mode squeezed vacuum state [25].

$$|\Psi\rangle = \frac{1}{\cosh(r)} \sum_{n,l}^{\infty} (-1)^{n+1} e^{i(n\theta_1 + l\theta_2)} \left(\frac{r_1}{r}\tanh(r)\right)^n \left(\frac{r_2}{r}\tanh(r)\right)^l \sqrt{\frac{(n+l)!}{n!l!}} |n, n+l, l\rangle_{s_1,i,s_2} \tag{1}$$

where r_1 and r_2 are the squeezing factors, $r = \sqrt{r_1^2 + r_2^2}$, and θ_1 and θ_2 are the phase terms.

The first task is to rewrite $\cosh(r)$ and $\tanh(r)$ in terms of the mean photon number per mode as is commonly done for the bipartite two mode squeezed light frequently used in quantum radar analysis [1, 2, 4, 13, 17]. In our case however, each branch will, in general, be a different mean photon number per mode, which we denote as N_{s_1}, N_{s_2}, and N_i for signal 1, signal 2, and the idler respectively. This allows for the covariance to be more directly comparable to the power level of each beam because these values directly relate to the amount of photons transmitted.

Since the tripartite implementation consists of three beams, there are multiple combinations of beams one can keep at the radar and send into free space. We propose the following system which uses two of the photon paths as signals and one of the photon paths as an idler. The reasoning behind this choice is to send as much energy into the free space path as possible to increase transmit power. We also choose to use the electric field which corresponds to the use of balanced homodyne detection.

First, the evaluation of the mean idler photon number, $N_i = \hat{a}_i^\dagger \hat{a}_i$:

$$\langle\Psi|\hat{a}_i\hat{a}_i^\dagger|\Psi\rangle = \frac{1}{\cosh^2(r)} \sum_{m,k}^{\infty}\sum_{n,l}^{\infty} e^{i(n\theta_1+l\theta_2)}e^{-i(m\theta_1+k\theta_2)} \left(\frac{r_1^{n+m}}{r^2}\tanh^{(n+m)}(r)\right)\left(\frac{r_2^{l+k}}{r^2}\tanh^{(l+k)}(r)\right) \times \sqrt{\frac{(n+l)!}{n!l!}}\sqrt{\frac{m!+k!}{m!k!}}(n+l)\langle m, m+k, k|n, n+l, l\rangle \quad (2)$$

Orthogonality causes $m = n$ and $k = l$ which yields:

$$\langle\Psi|\hat{a}_i\hat{a}_i^\dagger|\Psi\rangle = \frac{1}{\cosh^2(r)} \sum_{n,l=0}^{\infty} \tanh^{2(n+l)}(r)\frac{(n+l)!}{n!l!}\frac{r_1^{2n}r_2^{2l}}{r^{2(n+l)}}(n+l) \quad (3)$$

The above double summation can be evaluated by first applying different values of n to the formula, then evaluating the resulting sums over l. Doing this for the first few values of n gives (denoting each partial sum as F_n):

$$\begin{aligned} F_0 &= \frac{r^2\text{sech}^2(r)r_2^2\tanh^2(r)}{(r^2 - r_2^2\tanh^2(r))^2} \\ F_1 &= \frac{r^2\text{sech}^2(r)r_1^2(r^2\tanh^2(r) + r_2^2\tanh^4(r))}{(r^2 - r_2^2\tanh^2(r))^3} \\ F_2 &= \frac{r^2\text{sech}^2(r)r_1^4(2r^2\tanh^4(r) + r_2^2\tanh^6(r))}{(r^2 - r_2^2\tanh^2(r))^4} \\ F_3 &= \frac{r^2\text{sech}^2(r)r_1^6(3r^2\tanh^6(r) + r_2^2\tanh^8(r))}{(r^2 - r_2^2\tanh^2(r))^5} \end{aligned} \quad (4)$$

Given the above pattern of partial sums, the general formula is found to be:

$$\langle\Psi|\hat{a}_i\hat{a}_i^\dagger|\Psi\rangle = \frac{r^2}{\cosh^2(r)}\sum_{i=0}^{\infty}\frac{1}{(r^2 - r_2^2\tanh^2(r))^{(i+2)}}r_1^{2i}\left(ir^2\tanh^{2i}(r) + r_2^2\tanh^{2(i+1)}(r)\right) \quad (5)$$

The above sum can be evaluated and yields:

$$\langle\Psi|\hat{a}_i\hat{a}_i^\dagger|\Psi\rangle = N_i = \sinh^2(r) \quad (6)$$

Next, the mean photon number per mode of one of the signal beams is evaluated in a similar manner as the previous case, which yields:

$$\langle\Psi|\hat{a}_{s_1}\hat{a}_{s_1}^\dagger|\Psi\rangle = N_{s_1} = \frac{\sinh^2(r)r_2^2}{r^2} \quad (7)$$

Furthermore, evaluating $\hat{a}_{s_2}\hat{a}_{s_2}^\dagger$ in a similar manner gives:

$$\langle\Psi|\hat{a}_{s_2}\hat{a}_{s_2}^\dagger|\Psi\rangle = N_{s_2} = \frac{\sinh^2(r)r_1^2}{r^2} \quad (8)$$

In order to write $\tanh(r)$ and $\cosh(r)$ in terms of N_i, N_{s_1}, and N_{s_2}, we start by solving Equation (6) for $\cosh(r)$:

$$N_i = \sinh^2(r) = \cosh^2(r) - 1 \rightarrow \cosh(r) = \sqrt{N_i + 1} \quad (9)$$

We then solve for $\tanh(r)$ by dividing Equation (6) by Equation (9) which yields:

$$\sqrt{\frac{N_iN_{s_1}r^2}{N_i^2r_2^2 + N_{s_1}r^2}} = \tanh(r) \quad (10)$$

One can also obtain this result in reference to the other signal beam by dividing Equation (6) by Equation (8):

$$\sqrt{\frac{N_i N_{s_2} r^2}{N_i^2 r_1^2 + N_{s_2} r^2}} = \tanh(r) \tag{11}$$

Using the terms found for $\tanh(r)$ in (10) and for $\cosh(r)$ in (9), we can now write the wave function in terms of the mean photon number per modes for the paths:

$$\begin{aligned} |\Psi\rangle =& \frac{1}{\sqrt{N_i+1}} \sum_{n,l}^{\infty} (-1)^{n+1} e^{i(n\theta_1 + l\theta_2)} \left(\frac{r_1}{r} \times \sqrt{\frac{N_i N_{s_1} r^2}{N_i^2 r_2^2 + N_{s_1} r^2}} \right)^n \left(\frac{r_2}{r} \sqrt{\frac{N_i N_{s_1} r^2}{N_i^2 r_2^2 + N_{s_1} r^2}} \right)^l \\ & \times \sqrt{\frac{(n+l)!}{n!l!}} |n, n+l, l\rangle_{s_1,i,s_2} \end{aligned} \tag{12}$$

where we will set $\alpha = \frac{1}{\sqrt{N_i+1}}$ and $\beta(r) = \sqrt{\frac{N_i N_{s_1} r^2}{N_i^2 r_2^2 + N_{s_1} r^2}}$, making the wave function:

$$|\Psi\rangle = \alpha \sum_{n,l}^{\infty} (-1)^{n+1} e^{i(n\theta_1 + l\theta_2)} \left(\frac{r_1}{r} \beta(r) \right)^n \left(\frac{r_2}{r} \beta(r) \right)^l \sqrt{\frac{(n+l)!}{n!l!}} |n, n+l, l\rangle_{s_1,i,s_2} \tag{13}$$

2.2. Covariance Matrix

Now that we have obtained for the wave function in terms of the mean photon number per modes for the individual beams, we can now calculate the terms in the covariance matrix, namely:

$$V = \begin{pmatrix} \langle E_i^2 \rangle & \langle E_i E_{R_1} \rangle & \langle E_i E_{R_2} \rangle \\ \langle E_{R_1} E_i \rangle & \langle E_{R_1}^2 \rangle & \langle E_{R_1} E_{R_2} \rangle \\ \langle E_{R_2} E_i \rangle & \langle E_{R_2} E_{R_1} \rangle & \langle E_{R_2}^2 \rangle \end{pmatrix} \tag{14}$$

where E_x is the electric field operator for the idler, first signal path, or second signal path ($x = i$, s_1, and s_2 respectively) defined by [26]:

$$E(r,t) = \sum_{\mathbf{k}} \hat{\epsilon}_{\mathbf{k}} \mathcal{E}_{\mathbf{k}} a_{\mathbf{k}} e^{-i\chi} + \hat{\epsilon}_{\mathbf{k}} \mathcal{E}_{\mathbf{k}} a_{\mathbf{k}}^{\dagger} e^{i\chi} \tag{15}$$

where $\hat{a}_{\mathbf{k}}$ is the frequency mode's creation operator; $\mathbf{k}$ is the wave vector; and χ is the phase (which we can suppress by assuming that the signal and idler are aligned in time and space via shifting the data or using a delay line), $\hat{\epsilon}_{\mathbf{k}}$ is a unit polarization vector, given by

$$\mathcal{E}_{\mathbf{k}} = \left(\frac{\hbar \nu_{\mathbf{k}}}{2\epsilon_0 V} \right)^{\frac{1}{2}} \tag{16}$$

where $\hbar$ is the Planck's constant divided by 2π; $\nu_{\mathbf{k}}$ is the frequency associated with the momentum mode $\mathbf{k}$; ϵ_0 is the permittivity of free space; and V is the quantization volume. $\mathcal{E}_{\mathbf{k}}$ will be suppressed since it will be canceled in the final correlation calculations due to the fact these correlations are normalized. This will allow for greater calculation simplicity and easier to understand solutions. The integral formalism is also not required for the solution as we assume the field is approximately monochromatic (a single momentum mode) where future work will look at a full band signal. For an aligned signal and idler measurement with a linear polarization, Equation (15) reduces to:

$$\hat{E} = \hat{a} + \hat{a}^{\dagger} \tag{17}$$

It should be noted that the physically realizable version of these calculations is a tensor product between Equation (1) and the thermal noise state. Formally, this calculation is done with a density

matrix approach [5, 27], where we first determine the density matrix for the coupled three-mode squeezed vacuum state:

$$\rho_{CTSV} = \frac{1}{\cosh^2(r)} \sum_{n,l,m,k}^{\infty} (-1)^{n+m+2} e^{i(n\theta_1+l\theta_2)} e^{-i(m\theta_1+k\theta_2)} \times \left(\frac{r_1}{r}\beta(r)\right)^{m+n} \left(\frac{r_2}{r}\beta(r)\right)^{l+k} \sqrt{\frac{(n+l)!}{n!l!}} \sqrt{\frac{(m+k)!}{m!k!}} |n, n+l, l, j\rangle\langle m, m+k, k, j| \tag{18}$$

and the density matrix for the thermal noise state [27, 28]:

$$\rho_T = \frac{1}{N_T+1} \sum_i \left(\frac{N_T}{N_T+1}\right)^i |i\rangle\langle i| \tag{19}$$

where N_T is the mean photon number of the thermal state. The return density matrix is defined as:

$$\rho_{return} = \rho_{CTSV} \otimes \rho_T = \frac{1}{\cosh^2(r)} \frac{1}{N_T+1} \sum_{n,l,m,k}^{\infty} (-1)^{n+m+2} e^{i(n\theta_1+l\theta_2)} e^{-i(m\theta_1+k\theta_2)} \times \left(\frac{r_1}{r}\tanh(r)\right)^{m+n} \left(\frac{r_2}{r}\tanh(r)\right)^{l+k} \sqrt{\frac{(n+l)!}{n!l!}} \sqrt{\frac{(m+k)!}{m!k!}} |n, n+l, l, i, j\rangle\langle m, m+k, k, i, j| \tag{20}$$

which can be shown to be approximately valid in the high-noise regime.

The evaluation begins by looking at the on-diagonal terms for this matrix, which amounts to the variance of the respective beams. Beginning with the E_i^2 term:

$$E_i^2 = \hat{a}_i^2 + \hat{a}_i\hat{a}_i^\dagger + \hat{a}_i^\dagger\hat{a}_i + \hat{a}_i^{\dagger 2} \tag{21}$$

where, due to the orthogonality of the Fock State basis, the non-zero terms are found to be $\hat{a}_i\hat{a}_i^\dagger$ and $\hat{a}_i^\dagger\hat{a}_i$. We begin evaluating these non-zero terms starting with the $\hat{a}_i\hat{a}_i^\dagger$ term where again using the same methods of previous calculations, we find:

$$E_i^2 = \frac{\alpha^2(1+\beta(r)^2)}{(-1+\beta(r)^2)^2} \tag{22}$$

Now we will look at the two signal paths beginning with $E_{s_1}^2$. These terms differ from the idler path because the signal paths will have an added noise terms as these beams propagate in free space.

$$\begin{aligned} E_{R_1} =& \sqrt{\kappa}(\hat{a}_{s_1} + \hat{a}_{s_1}^\dagger) + \sqrt{1-\kappa}(\hat{a}_{B_1} + \hat{a}_{B_1}^\dagger) \\ E_{R_1}^2 =& \kappa\left(\hat{a}_{s_1}^2 + \hat{a}_{s_1}^{2\dagger} + a_{s_1}a_{s_1}^\dagger + a_{s_1}^\dagger a_{s_1}\right) + (1-\kappa)\left(a_{B_1}^2 + a_{B_1}^{\dagger 2} + a_{B_1}a_{B_1}^\dagger + a_{B_1}^\dagger a_{B_1}\right) \\ &+ \sqrt{\kappa(1-\kappa)}\left(\hat{a}_{s_1}\hat{a}_{B_1} + \hat{a}_{s_1}^\dagger\hat{a}_{B_1}^\dagger + \hat{a}_{s_1}\hat{a}_{B_1}^\dagger + \hat{a}_{s_1}^\dagger\hat{a}_{B_1} + \hat{a}_{B_1}\hat{a}_{s_1} + \hat{a}_{B_1}^\dagger\hat{a}_{s_1}^\dagger + \hat{a}_{B_1}\hat{a}_{s_1}^\dagger + \hat{a}_{B_1}^\dagger\hat{a}_{s_1}\right) \end{aligned} \tag{23}$$

where a_{s_1}, a_{s_2}, and a_B are the field mode operators for signal 1, signal 2, and the noise state, respectively. Using the orthogonality conditions we determine that the only non-zero terms are $\hat{a}_{s_1}^\dagger\hat{a}_{s_1}$, $\hat{a}_{s_1}\hat{a}_{s_1}^\dagger$, $\hat{a}_{B_1}^\dagger\hat{a}_{B_1}$, and $\hat{a}_{B_1}\hat{a}_{B_1}^\dagger$ where the coefficients generated from the evaluation of the expectation creation and annihilation operators are $n+1$, n, $N_{B_1}+1$, and N_B respectively. Therefore the expectation value to be evaluated composed of non-zero terms takes the form:

$$\langle\Psi|\hat{a}_{s_1}^\dagger\hat{a}_{s_1} + \hat{a}_{s_1}\hat{a}_{s_1}^\dagger + \hat{a}_{B_1}\hat{a}_{B_1}^\dagger + \hat{a}_{B_1}^\dagger\hat{a}_{B_1}|\Psi\rangle \tag{24}$$

Using this, the variance term of the first signal path is found to be:

$$\langle\Psi|E_{R_1}^2|\Psi\rangle = \frac{\alpha^2((1+\beta(r)^2(-1+\kappa-2N_{B_2})+2N_{B_2})r^2 + \beta(r)^2\kappa(r_1^2-r_2^2))}{(-1+\beta(r)^2)^2r^2} \tag{25}$$

Similarly, the variance term of the second signal path is found to be:

$$\langle\Psi|E_{R_2}^2|\Psi\rangle = \frac{\alpha^2((1+\beta(r)^2(-1+\kappa-2N_{B_2})+2N_{B_2})r^2 + \beta(r)^2\kappa(-r_1^2+r_2^2))}{(-1+\beta(r)^2)^2r^2} \tag{26}$$

Now we will look at the first cross-correlation term in our covariance matrix, but first it should be noted that the final covariance matrix is simplified because it can be shown that the electric fields between branches commute due to the differing mode operator commutators.

This allows us to simply solve for only three cross-correlation terms instead of the six that are in the matrix; in other words, the covariance matrix is symmetric.

We now determine $E_{R_1}E_{R_2}$, where we again use the orthonormality of the Fock state basis to find the non-zero terms. These terms are found to be $\hat{a}^\dagger_{s_1}\hat{a}_{s_2}$ and $\hat{a}_{s_1}\hat{a}^\dagger_{s_2}$ with coefficients $\kappa\sqrt{l(n+1)}$ and $\kappa\sqrt{n(l+1)}$ respectively. Where we first evaluate $\hat{a}_{s_1}\hat{a}^\dagger_{s_2}$:

$$\langle\Psi|\hat{a}_{s_1}\hat{a}^\dagger_{s_2}|\Psi\rangle = \kappa\alpha^2\sum_{l=0}^{\infty}\beta(r)^{2(n+l)}\frac{(n+l)!}{n!l!}\frac{r_1^{2n}r_2^{2l}}{r^{2(n+l)}}\sqrt{l(n+1)} \tag{27}$$

we also see that the function for $\hat{a}^\dagger_{s_1}\hat{a}_{s_2}$ is:

$$\langle\Psi|\hat{a}^\dagger_{s_1}\hat{a}_{s_2}|\Psi\rangle = \kappa\alpha^2\sum_{l=0}^{\infty}\beta(r)^{2(n+l)}\frac{(n+l)!}{n!l!}\frac{r_1^{2n}r_2^{2l}}{r^{2(n+l)}}\sqrt{n(l+1)} \tag{28}$$

These equations are not able to be solved trivially using the methods from Equations (2) to (4). To solve this, we must numerically calculate the resulting expressions because it does not have a closed form evaluation of the sums. We use the above results together to write:

$$\langle\Psi|E_{s_1}E_{s_2}|\Psi\rangle = \kappa\alpha^2\sum_{n,l=0}^{\infty}\Xi(n,l)\sqrt{n(l+1)}+\sqrt{l(n+1)} \tag{29}$$

where we have defined:

$$\Xi(n,l) = \beta(r)^{2(n+l)}\frac{(n+l)!}{n!l!}\frac{r_1^{2n}r_2^{2l}}{r^{2(n+l)}} \tag{30}$$

We now evaluate $E_{s_1}E_i$, where again the signal has an added noise term:

$$\begin{aligned}
E_{R_1} =&\sqrt{\kappa}(\hat{a}_{s_1}+\hat{a}^\dagger_{s_1})+\sqrt{1-\kappa}(\hat{a}_{B_1}+\hat{a}^\dagger_{B_1})\\
E_i =&\hat{a}_i+\hat{a}^\dagger_i\\
E_{R_1}E_i =&\sqrt{\kappa}\hat{a}_{s_1}\hat{a}_i+\sqrt{\kappa}\hat{a}^\dagger_{s_1}\hat{a}_i+\sqrt{\kappa}\hat{a}_{s_1}\hat{a}^\dagger_i+\sqrt{\kappa}\hat{a}^\dagger_{s_1}\hat{a}^\dagger_i\\
&+\sqrt{1-\kappa}\hat{a}_{B_1}\hat{a}_i+\sqrt{1-\kappa}\hat{a}^\dagger_{B_1}\hat{a}_i+\sqrt{1-\kappa}\hat{a}_{B_1}\hat{a}^\dagger_i+\sqrt{1-\kappa}\hat{a}^\dagger_{B_1}\hat{a}^\dagger_i
\end{aligned} \tag{31}$$

We again use a general formula to solve this similar to Equation (4) and find the solution to be:

$$\langle\Psi|E_{s_1}E_i|\Psi\rangle = \kappa\alpha^2\sum_{n,l=0}^{\infty}\Xi(n,l)\left(\sqrt{n(n+l)}+\sqrt{(n+1)(n+l+1)}\right)$$

Finally, we calculate $E_{s_2}E_i$ and determine it to be:

$$\langle\Psi|E_{s_2}E_i|\Psi\rangle = \kappa\alpha^2\sum_{n,l=0}^{\infty}\Xi(n,l)\left(\sqrt{l(n+l)}+\sqrt{(l+1)(n+l+1)}\right) \tag{32}$$

Combining the solutions to these terms and putting them into the covariance matrix discussed earlier, we obtain the matrix seen in Equation (33).

$$V = \begin{pmatrix}\langle E_i^2\rangle & \langle E_iE_{s_1}\rangle & \langle E_iE_{s_2}\rangle\\ \langle E_{s_1}E_i\rangle & \langle E_{s_1}^2\rangle & \langle E_{s_1}E_{s_2}\rangle\\ \langle E_{s_2}E_i\rangle & \langle E_{s_2}E_{s_1}\rangle & \langle E_{s_2}^2\rangle\end{pmatrix} \tag{33}$$

where for the ease of reading, the elements of the matrix are listed below in Equation (34):

$$E_i^2 = \frac{\alpha^2(1+\beta(r)^2)}{(-1+\beta(r)^2)^2}$$

$$E_{s_1}^2 = \frac{\alpha^2((1+\beta(r)^2(-1+\kappa-2N_{B_1})+2N_{B_1})r^2+\beta(r)^2\kappa(r_1^2-r_2^2))}{(-1+\beta(r)^2)^2r^2}$$
$$E_{s_2}^2 = \frac{\alpha^2((1+\beta(r)^2(-1+\kappa-2N_{B_2})+2N_{B_2})r^2+\beta(r)^2\kappa(-r_1^2+r_2^2))}{(-1+\beta(r)^2)^2r^2}$$
$$E_{s_1}E_i = \kappa\alpha^2\sum_{n,l=0}^{\infty}\Xi(n,l)\left(\sqrt{n(n+l)}+\sqrt{(n+1)(n+l+1)}\right)$$
$$E_{s_1}E_{s_2} = \kappa\alpha^2\sum_{n,l=0}^{\infty}\Xi(n,l)\left(\sqrt{n(l+1)}+\sqrt{l(n+1)}\right)$$
$$E_{s_2}E_i = \kappa\alpha^2\sum_{n,l=0}^{\infty}\Xi(n,l)\left(\sqrt{l(n+l)}+\sqrt{(l+1)(n+l+1)}\right) \tag{34}$$

3. ANALYSIS

Now that the tripartite covariance matrices have been derived, we plot the correlations at various transmissivities in Figure 1. These correlations are solved using the covariances and variances, σ:

$$r_{xy} = \frac{\mathrm{cov}(x,y)}{\sqrt{\sigma_x^2\sigma_y^2}} \tag{35}$$

where the horizontal and vertical axes are r_1 and r_2, respectively. Here one can see that the correlations between the idler and the individual signal paths are higher than just the signal paths. This may be due to the idler being created through a mixing of the signal paths and the signal paths being created through independent lasers.

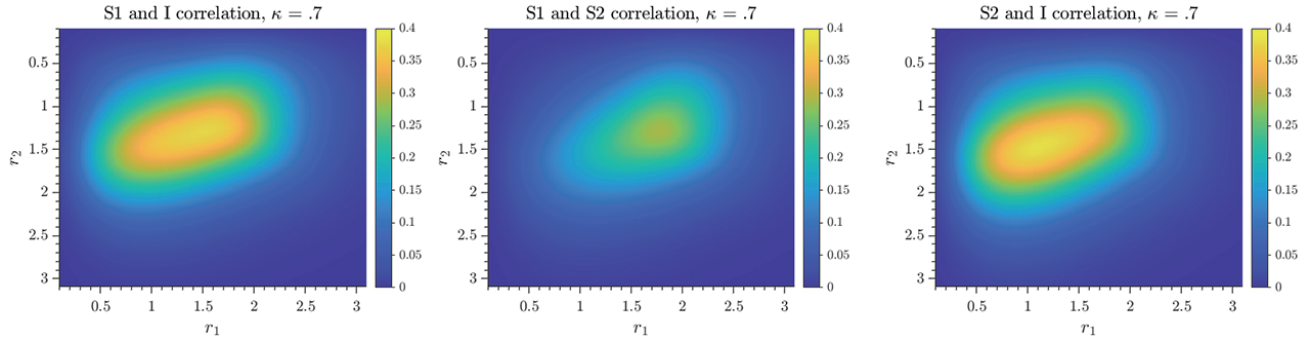

Figure 1. Correlations of the three path combinations in terms of r_1 and r_2, $N_B = 10$.

Next, we define a detector function that will allow for the system to yield the best possible performance. This detector function is designed to keep the two signals together and correlate them both with the idler at the same time.

To define this system mathematically, we begin with the formula to determine the correlation shown in Equation (35) and applying the tripartite system we obtain the detector function:

$$r_{df} = \frac{\langle(E_{s_1}+E_{s_2})E_i\rangle}{\sqrt{\langle E_i^2\rangle\langle E_{s_1}^2+E_{s_2}^2+E_{s_1}E_{s_2}\rangle}} \tag{36}$$

where each part of this function has been previously solved and is plotted in Figure 2 at $\kappa = .07$, .4, and .7. One can see that as the environment becomes more transmissive (i.e., higher κ), the correlation increases. One can also see that based on the correlations determined from the detector function,

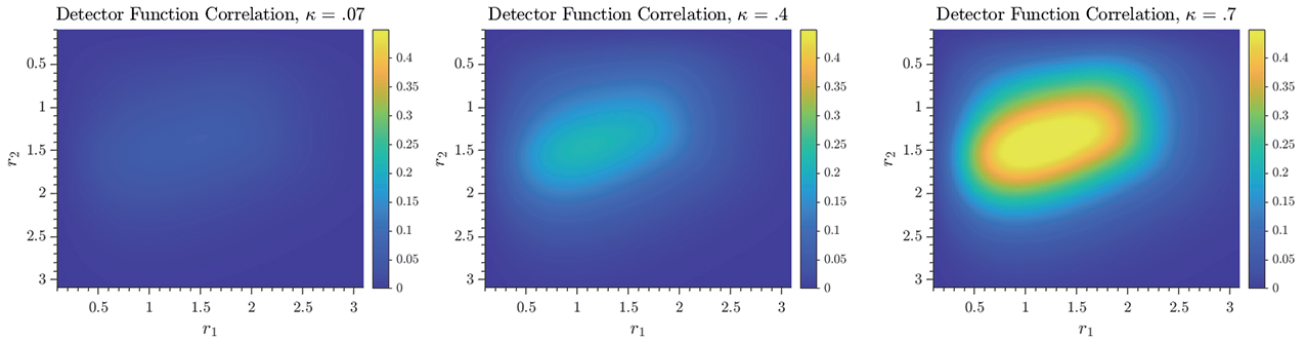

Figure 2. Correlations for for the tripartite system using the detector function at various transmissivities, $N_B = 10$.

changing r_1 independently does not have the same effect on the correlation as r_2. Due to this and the relationship between the individual squeezing factors, one value of N_s can have multiple different correlations. For example, $r_1 = 1.5$ and $r_2 = 1$ have a different correlation from $r_1 = 1$ and $r_2 = 1.5$, but will have the same N_s. To alleviate these degeneracies in the plot, we show the case where $r_1 = r_2$ in Figure 3 where it is plotted in comparison to the known bipartite correlation coefficient [24]. One can see that much like current quantum radar systems, the system is more effective at lower signal powers; however, compared to the bipartite system, it does not obtain as high of a correlation. One can also see that the bipartite system continues at higher N_s to have the high correlation, while the tripartite system falls off at high N_s, which again may be due to how N_s is defined. This means that for the tripartite system there is a finite region of significant correlation and increasing the squeezing factor does not always increase the correlation, while the bipartite system continues increasing as the squeezing factor increases until the correlation becomes 1.

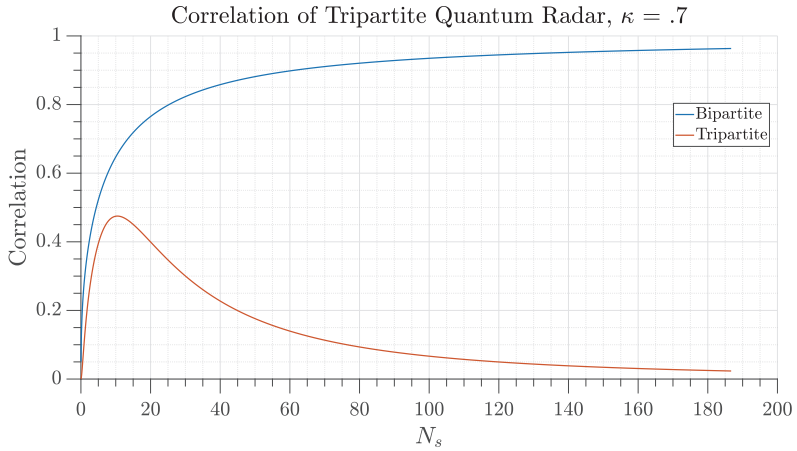

Figure 3. Correlations for the tripartite system when $r_1 = r_2$ versus the bipartite system, N_B=10.

4. CONCLUSION

In this paper we derived the electric field covariance matrix for the tripartite quantum radar system. We then showed that with a combined electric field measurement we are able to obtain correlations between the different beam paths where, like bipartite quantum radar, the correlations are higher at lower power. However, at higher power levels, these correlations seem to fall off.

From these correlations, it was found that all three paths have correlations with each other which could be useful in creating new detection functions that could be used within a radar or quantum

communication system to prevent eavesdropping and increase security.

Overall it seems that the tripartite quantum system is viable for use in correlation based tasks, but lacks in comparison to the current two photon systems. Although, due to the addition of the third photon, a tripartite system may be able to obtain higher N_s compared to the bipartite system.

ACKNOWLEDGMENT

This work is a collaborative effort between the Pennsylvania State Applied Research Laboratory and the Naval Engineering Education Consortium (NEEC) through NEEC Grant # N00174-19-1-0007 awarded by the Naval Surface Warfare Center, Crane Division.

REFERENCES

1. Bowell, R. A., M. J. Brandsema, B. M. Ahmed, R. M. Narayanan, S. W. Howell, and J. M. Dilger, "Electric field correlations in quantum radar and the quantum advantage," *Proc. SPIE Conference on Radar Sensor Technology XXIV*, On-line, Vol. 11408, Apr. 2020, doi: 10.1117/12.2562749.
2. Brandsema, M. J., R. M. Narayanan, and M. Lanzagorta, "Correlation properties of single photon binary waveforms used in quantum radar/lidar," *Proc. SPIE Conference on Radar Sensor Technology XXIV*, On-line, Vol. 11408, Apr. 2020, doi: 10.1117/12.2560184.
3. Chang, C. W. S., A. M. Vadiraj, J. Bourassa, B. Balaji, and C. M. Wilson, "Quantum-enhanced noise radar," *Applied Physics Letters*, Vol. 114, No. 11, 112601, Mar 2019.
4. Lanzagorta, M., *Quantum Radar*, Morgan & Claypool, San Rafael, CA, USA, 2011.
5. Guha, S. and B. I. Erkmen, "Gaussian-state quantum illumination receivers for target detection," *Physical Review A*, Vol. 80, No. 5, 052310, Nov. 2009.
6. Shapiro, J. H., "The quantum illumination story," *IEEE Aerospace and Electronic Systems Magazine*, Vol. 35, No. 4, 8–20, Apr. 2020.
7. Lanzagorta, M., "Low-brightness quantum radar," *Proc. SPIE Conference on Radar Sensor Technology XIX and Active and Passive Signatures VI*, Vol. 9461, Baltimore, MD, Apr. 2015, doi: 10.1117/12.2177577.
8. Luong, D., C. S. Chang, A. Vadiraj, A. Damini, C. Wilson, and B. Balaji, "Receiver operating characteristics for a prototype quantum two-mode squeezing radar," *IEEE Transactions on Aerospace and Electronic Systems*, Vol. 56, No. 3, 2041–2060, Jun. 2020.
9. Lopaeva, E. D., I. Ruo Berchera, I. Degiovanni, S. Olivares, G. Brida, and M. Genovese, "Experimental realization of quantum illumination," *Physical Review Letters*, Vol. 110, No. 15, 153603, Apr. 2013.
10. Barzanjeh, S., S. Guha, C. Weedbrook, D. Vitali, J. H. Shapiro, and S. Pirandola, "Microwave quantum illumination," *Physical Review Letters*, Vol. 114, No. 8, 080503, Feb. 2015.
11. Zhang, Z., S. Mouradian, F. N. Wong, and J. H. Shapiro, "Entanglement-enhanced sensing in a lossy and noisy environment," *Physical Review Letters*, Vol. 114, No. 11, 110506, Mar. 2015.
12. Luong, D., S. Rajan, and B. Balaji, "Quantum two-mode squeezing radar and noise radar: Correlation coefficients for target detection," *IEEE Sensors Journal*, Vol. 20, No. 10, 5221–5228, May 2020.
13. Luong, D., B. Balaji, and S. Rajan, "Biomedical sensing using quantum radars based on Josephson parametric amplifiers," *Proc. 2021 International Applied Computational Electromagnetics Society Symposium (ACES)*, Hamilton, ON, Aug. 2021, doi: 10.1109/ACES53325.2021.00091.
14. Liu, H., B. Balaji, and A. S. Helmy, "Target detection aided by quantum temporal correlations: Theoretical analysis and experimental validation," *IEEE Transactions on Aerospace and Electronic Systems*, Vol. 56, No. 5, 3529–3544, Oct. 2020.
15. Yang, H., W. Roga, J. D. Pritchard, and J. Jeffers, "Gaussian state-based quantum illumination with simple photodetection," *Optics Express*, Vol. 29, No. 6, 8199–8215, Mar. 2021.
16. England, D. G., B. Balaji, and B. J. Sussman, "Quantum-enhanced standoff detection using correlated photon pairs," *Physical Review A*, Vol. 99, 023828, Feb. 2019.

17. Guha, S., "Receiver design to harness the quantum illumination advantage," *Proc. 2009 IEEE International Symposium on Information Theory (ISIT)*, Seoul, Korea, 963–967, Jun.–Jul. 2009.
18. Zhuang, Q., and J. H. Shapiro, "Ultimate accuracy limit of quantum pulse-compression ranging," arXiv:2109.11079v1, Sep. 2021.
19. Blakely, J. N., "Bounds on probability of detection error in quantum-enhanced noise radar," *Quantum Reports*, Vol. 2, No. 3, 400–413, Jul. 2020.
20. Tan, S.-H., B. I. Erkmen, V. Giovannetti, S. Guha, S. Lloyd, L. Maccone, S. Pirandola, and J. H. Shapiro, "Quantum illumination with Gaussian states," *Physical Review Letters*, Vol. 101, No. 25, 253601, Dec. 2008.
21. Dawood, M. and R. M. Narayanan, "Receiver operating characteristics for the coherent UWB random noise radar," *IEEE Transactions on Aerospace and Electronic Systems*, Vol. 37, No. 2, 586–594, Apr. 2001.
22. Russer, J. A., M. Würth, W. Utschick, F. Bischeltsrieder, and M. Peichl, "Performance considerations for quantum radar," *Proc. 2021 International Applied Computational Electromagnetics Society Symposium (ACES)*, Hamilton, ON, Aug. 2021, doi: 10.1109/ACES53325.2021.00105.
23. Bowell, R. A., M. J. Brandsema, R. M. Narayanan, S. W. Howell, and J. M. Dilger, "Tripartite correlation performance for use in quantum radar systems," *Proc. SPIE Conference on Radar Sensor Technology XV*, On-line, Vol. 11742, Apr. 2021, doi: 10.1117/12.2588308.
24. Bowell, R. A., M. J. Brandsema, R. M. Narayanan, S. W. Howell, and J. M. Dilger, "Comparison of correlation performance for various measurement schemes in quantum bipartite radar and communication systems," *Progress In Electromagnetics Research*, Vol. 174, 43–53, 2022.
25. Zhang, W. and R. T. Glasser, "Coupled three-mode squeezed vacuum," arXiv:2002.00323v1, 2020.
26. Scully, M. O. and M. S. Zubairy, *Quantum Optics*, Cambridge, UK, Cambridge University Press, 1997.
27. Vourdas, A., "Optical signals with thermal noise," *Physical Review A*, Vol. 39, No. 1, 206–213, Jan. 1989.
28. Helstrom, C. W., *Quantum Detection and Estimation Theory*, Academic Press, New York, NY, USA, 1976.